

Cost-Free Personalization via Information-Geometric Projection in Bayesian Federated Learning

Nour Jamoussi
EURECOM
France
jamoussi@eurecom.fr

Giuseppe Serra
EURECOM
France
serra@eurecom.fr

Photios A. Stavrou
EURECOM
France
stavrou@eurecom.fr

Marios Kountouris
University of Granada, Spain
EURECOM, France
mariosk@ugr.es

Abstract

Bayesian Federated Learning (BFL) combines uncertainty modeling with decentralized training, enabling the development of personalized and reliable models under data heterogeneity and privacy constraints. Existing approaches typically rely on Markov Chain Monte Carlo (MCMC) sampling or variational inference, often incorporating personalization mechanisms to better adapt to local data distributions. In this work, we propose an information-geometric projection framework for personalization in parametric BFL. By projecting the global model onto a neighborhood of the user’s local model, our method enables a tunable trade-off between global generalization and local specialization. Under mild assumptions, we show that this projection step is equivalent to computing a barycenter on the statistical manifold, allowing us to derive closed-form solutions and achieve cost-free personalization. We apply the proposed approach to a variational learning setup using the Improved Variational Online Newton (IVON) optimizer and extend its application to general aggregation schemes in BFL. Empirical evaluations under heterogeneous data distributions confirm that our method effectively balances global and local performance with minimal computational overhead.

1. Introduction

Federated learning (FL) is a collaborative machine learning paradigm designed to preserve data privacy. By connecting a central server to multiple participants, commonly referred to as clients or end-users, FL enables distributed training while keeping data local to the clients. In general,

FL algorithms operate by training local models on the private datasets of clients and aggregating these models into a global model maintained on the server. After performing local updates, clients share their updated model parameters with the server, which aggregates them to refine the global model. The updated global model is then sent back to the clients for further local training [37].

In real-world scenarios, statistical heterogeneity among clients is a frequent challenge. For example, variations in MRI machines across hospitals can result in feature skewness, where input data distributions differ significantly between clients. Similarly, label distribution shifts can arise when some clients have disproportionately more samples from certain classes compared to others. This often occurs in specialized hospitals dedicated to specific diseases, as opposed to general hospitals. Such heterogeneity violates the theoretical assumption of independent and identically distributed (i.i.d.) data, leading to significant performance degradation and increased uncertainty in the global model when evaluated on local test data.

Personalized Federated Learning (PFL) is a paradigm in which clients can adapt the global model to their local data, i.e., model personalization, with the objective of limiting the impact of statistical heterogeneity. In [45], the authors propose a distinctive taxonomy for PFL approaches, categorizing them into global model personalization techniques, e.g., client selection [49], meta-learning [18] and transfer-learning [9], and learning personalized models techniques, e.g., parameter decoupling [4], knowledge distillation [26] and clustering [42]. Furthermore, multiple studies [6, 32, 51, 52] applied Bayesian methods to the PFL framework, achieving better model calibration and uncertainty quantification. The transition from deter-

ministic FL to Bayesian FL (BFL) naturally leads to an investigation of the manifolds to which clients’ and global posteriors distributions belong, allowing for the exploration of their properties and the operations that can be defined on them, as suggested in [25].

In this work, we study the PFL paradigm through the lens of Bayesian learning, leveraging Information Geometry to develop a personalization method for BFL. Unlike existing approaches, our method does not require fine-tuning, additional training, or access to local or shared global data, making it a fully private and truly cost-free personalization technique. By specifying a divergence metric, we learn the personalized model posteriors by projecting the global model posterior distribution onto a sphere centered at the local model posterior distribution, where the radius encodes the desired degree of personalization the end-user would like to achieve. This method provides unlimited personalization flexibility, empowering end-users to seamlessly control the trade-off between local and global performance at no additional cost.

We show that for any divergence that is convex in its first argument, the projection problem is equivalent to computing the weighted barycenter of the local posterior and the global posterior distributions. This connection between two key concepts in Information Geometry, namely, geometric projection and the geometric barycenter, offers an interpretable link between the radius of the sphere and the weights for the barycentric aggregation. As a result, the degree of personalization becomes more intuitive and accessible to end-users.

The paper is structured as follows. Section 2 provides an extensive analysis of the related work. In Section 3, we present the parametric BFL framework based on variational learning for local training and posterior aggregation to determine the posterior global model. We propose a design that extends the prior use [40] of the Improved Variational Online Newton optimizer (IVON) [43] for various aggregation methods. In Section 4, we introduce the novel idea we present to personalize global BFL models using information-geometric projection and show its equivalence to barycentric aggregation for divergence functions convex in their first argument. Worth noting that the personalization method is not limited to parametric BFL, as the idea of personalization remains general and valid for the different settings of BFL, non-parametric included. Subsequently, we refine our results for the parametric case where, for specific divergences, we can leverage closed-form solutions for the barycenters, leading to substantial gains in algorithmic efficiency. We dedicate Section 5 to the experimental analysis, where we compare various aggregation techniques under the variational learning setting. Furthermore, we evaluate our method against state-of-the-art approaches and demonstrate that it achieves a favorable global/local trade-off com-

pared to existing baselines.

2. Background and Related Work

Bayesian Federated Learning BFL seeks to integrate the advantages of Bayesian Deep Learning, e.g., better model calibration and uncertainty quantification, within the FL framework. Following the classification proposed in [7], BFL approaches can be broadly categorized into two main types; Client-side BFL [5, 6, 23, 36, 51, 52] and server-side BFL [1, 8, 10, 22], with certain overlaps between these groups, reflecting the diversity in model formulations and inference techniques. In [25], the authors extend the discussion on the parametric client-side BFL framework by categorizing methods according to the techniques used to aggregate the local posteriors and propose a unified framework for aggregation rooted in Information Geometry.

However, for the scope of this work, it is useful to introduce an additional categorization of BFL based on the adopted modeling assumptions, distinguishing between parametric and nonparametric Bayesian methods.

- *Parametric BFL*: Parametric Bayesian learning constitutes a principled framework within Bayesian statistics, in which the data generation process is assumed to adhere to a parametric model. Specifically, this approach assumes that the data distribution can be fully characterized by a finite set of parameters. The parametric family most commonly considered in BFL is the Gaussian family, where both client-specific posteriors and the global model posterior are approximated using Gaussian distributions [22, 29, 39, 40, 44, 51]. This Gaussian assumption facilitates tractable inference and efficient parameter aggregation.
- *Nonparametric BFL*: Unlike parametric BL, nonparametric Bayesian learning doesn’t restrict the model to a specific family of distributions. Instead, it provides the flexibility to learn directly from the data, allowing the structure and complexity to emerge naturally rather than being predefined. This approach leverages distributions over infinite-dimensional function spaces, such as Gaussian Processes or Dirichlet Processes employed in the context of BFL in [50]. Additionally, Particle-Based VI, utilized in [27] for BFL, aligns with the non-parametric perspective by using a set of particles to approximate posteriors without assuming a predefined parametric family.

Personalized Bayesian Federated Learning Personalized BFL extends the standard BFL framework by incorporating client-specific adaptations to the shared global model. FedPop [32] captures this personalization by modeling each client’s data generation process as a combination of fixed shared population parameters, describing the common data model, and client-specific random effects, describing the

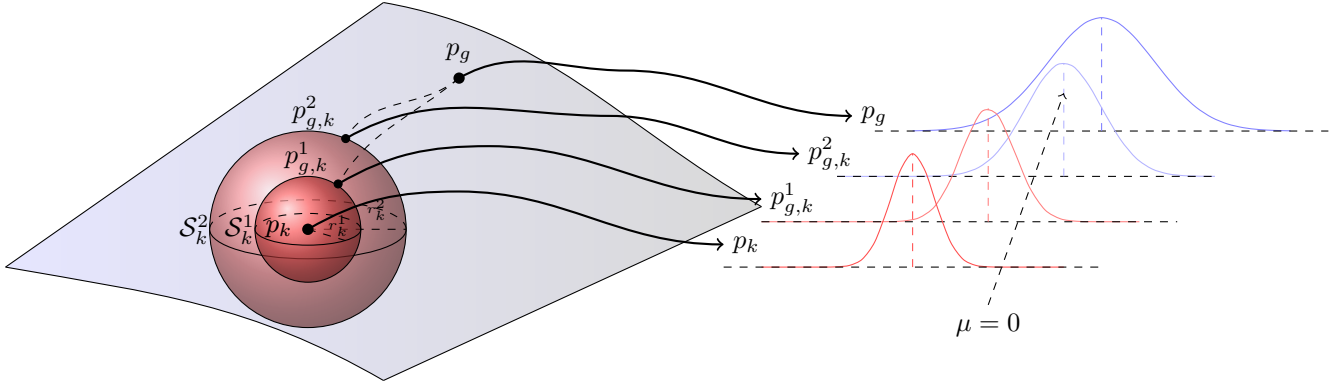


Figure 1. Personalization through information-geometric projection. The figure presents two projection scenarios illustrated with two local spheres \mathcal{S}_k^1 and \mathcal{S}_k^2 of increasing radius r_k^1 and r_k^2 , highlighting the impact of the radius on the closeness of the projected distribution to the global or local distribution.

heterogeneity in the clients’ data, thus providing personalization and uncertainty estimation capabilities. To infer these parameters efficiently, FedPop employs MCMC methods to approximate local posterior distributions and perform stochastic optimization in a federated setting. Although MCMC ensures flexible and asymptotically exact Bayesian inference, it can be computationally expensive in large-scale settings. To address this, pFedBayes [51] employs variational inference to approximate client-specific posteriors, optimizing a tractable Evidence Lower Bound (ELBO) to achieve computational efficiency in BFL. Although pFedBayes presents a promising approach to personalization in BFL, certain aspects of its methodology introduce notable limitations. Firstly, the degree of personalization is uniformly applied across all clients and determined empirically, without an adaptive mechanism or an intuitive explanation to tailor it to individual client characteristics. Secondly, it defines the local model as personalized based on the use of VI, where the global model serves as a prior within the KL divergence term of the ELBO. This formulation may be controversial within the Bayesian community, as the classical interpretation of a prior belief should be independent of the observed data. More recently, pFedVEM [52] has taken advantage of variational inference to estimate the specific uncertainty of the client and the deviation of the model, modeling the client parameters as Gaussian distributed around a global latent variable. It employs a confidence-based aggregation strategy that ensures that clients with lower uncertainty and fewer deviations contribute more to the global model.

Unlike the aforementioned methods, our approach presents personalization as an additional step independent from the training process, as it only requires access to the global and local posteriors with no need for extra data or fine-tuning. In addition, our approach allows access to three different variants of the model, i.e., local, personalized, and global

models, as suggested in [16], with the possibility of continually adjusting the personalized variant without additional training cost.

Information Geometry and Optimal Transport in FL

Information Geometry [3] provides a general framework for the study of the geometric properties of statistical manifolds when considering divergence functions, allowing us to intuitively treat distributions as elements in a manifold. This framework allows for the natural translation of fundamental geometric concepts, such as projections onto constraint sets [12, 13] and the identification of barycenters, serving as statistical centers of mass for a given set of probability distributions [17, 38].

On the other hand, Optimal Transport [46] focuses on identifying the most efficient transport plan between two probability distributions in terms of a given cost function. Under specific assumptions on the cost function, optimal transport allows one to define distance functions on the statistical manifold, as shown by the family of Wasserstein- p distances [46]. The Sinkhorn algorithm [14] serves as a natural bridge between Information Geometry and Optimal Transport, allowing for efficient computation of the transport plan by incorporating entropy regularization into the Optimal Transport problem.

Multi-Marginal Optimal Transport (MMOT) [21, 41] extends the classical two-marginal Optimal Transport problem to multiple distributions by seeking an optimal joint coupling that minimizes a given n -ary cost function of all marginal distributions. Furthermore, for specific cases of the n -ary cost, it can be shown that the MMOT problem is equivalent to the computation of the Wasserstein Barycenter (WB) of the set of marginals. This equivalence highlights the MMOT as a more general framework, within which the WB emerges as a special case, characterizing the optimal interpolation of multiple distributions in the Wasser-

stein space. Applications of concepts from the Information Geometry and Optimal Transport literature have recently been explored in the FL setting. In [19], the authors introduce FedOT, a PFL algorithm that integrates Optimal Transport with model training. FedOT employs deterministic FL, leveraging MMOT to align data distributions. Specifically, it learns transport maps to transform data points from heterogeneous distributions into a shared domain while simultaneously training a predictive model on the mapped data. In a similar approach, FedDRO [34] aggregates client data distributions via a Wasserstein barycenter and trains the global model against worst-case perturbations within a Wasserstein ball around this barycenter. In the context of BFL, [24] considers structured latent variable models by keeping local latent variables private, formulating a decentralized variational inference problem for which a communication-efficient aggregation based on Wasserstein barycenters is proposed. In [25], the authors propose a unifying framework for aggregation in BFL based on barycentric aggregation.

3. Parametric Bayesian Federated Learning

3.1. Learning Phase

The primary objective of BFL is to estimate the posterior distribution of the global model parameters, denoted as $p(\theta^*|\mathcal{D})$, utilizing the posterior distributions of local models, $p(\theta_k|\mathcal{D}_k)$. However, exact posterior inference is typically computationally intractable, often requiring the introduction of approximate inference methods. In this study, we adopt variational learning to approximate local posterior distributions based on a shared prior distribution $p(\theta)$ and client-specific likelihoods $p(\mathcal{D}_k|\theta_k)$. Given a parametric distribution family \mathcal{Q} , optimization seeks a distribution $q \in \mathcal{Q}$ that minimizes the KL divergence from the true posterior distribution $p(\theta|\mathcal{D})$, i.e.,

$$\min_{q(\theta) \in \mathcal{Q}} \text{D}_{\text{KL}}(q(\theta)||p(\theta|\mathcal{D})). \quad (1)$$

However, direct optimization of (1) remains challenging, leading to the adoption of the Negative Evidence Lower Bound (ELBO) as a surrogate objective

$$\min_{q(\theta) \in \mathcal{Q}} -\mathbb{E}_{q(\theta)}[\log p(\mathcal{D}|\theta)] + \text{D}_{\text{KL}}(q(\theta)||p(\theta)). \quad (2)$$

We approximate the posterior distributions of the local models $p(\theta_k|\mathcal{D}_k)$, $\forall k \in \{1, \dots, N\}$ by optimizing the objective (2) using the IVON optimizer [43] grounded in the Bayesian learning rule [28]. In contrast to classical variational inference, IVON integrates variational learning directly into the optimization process, without altering the model architecture or loss function. IVON maintains a Gaussian posterior over weights through efficient second-order updates based on reparameterized Hessian estimates, enabling

uncertainty-aware learning at a cost comparable to deterministic learning with Adam, thereby making Bayesian deep learning more scalable. Subsequently, these local posteriors are aggregated to obtain the global posterior distribution $p(\theta^*|\mathcal{D})$.

Based on this formulation, we introduce the following assumptions regarding the common prior $p(\theta)$ and the parametric family \mathcal{Q} , which will hold in our experimental setting presented in Section 5.

Assumption 1 (Mean-field Model). *The parametric family \mathcal{Q} consists of d -dimensional Gaussian distributions with independent marginals. Specifically, $\theta \sim \mathcal{N}(\mu, \Sigma)$, where $\mu \in \mathbb{R}^d$ is the mean vector and $\Sigma = \text{diag}(\sigma_1^2, \dots, \sigma_d^2)$ is a diagonal covariance matrix.*

3.2. Aggregation Phase

The aggregation phase refers to the process of combining locally trained model updates from multiple clients into a global model. In the following, we outline and discuss various aggregation techniques for the N local distributions, each consistent with Assumption 1 and parametrized with $\{(\mu_k, \Sigma_k)\}_{k=1}^N$.

- *Empirical Arithmetic Aggregation* employed in [5, 20, 39, 51], also known as naive aggregation, is the weighted average of the distribution statistics:

$$\Sigma_{EAA} = \sum_{k=1}^N w_k \Sigma_k, \quad \mu_{EAA} = \sum_{k=1}^N w_k \mu_k. \quad (3)$$

- *Barycentric Aggregation*, employed for BFL in [25], uses the barycenter of the clients' posteriors as an aggregated model, minimizing the average discrepancy across clients. Some examples include:

- The Wasserstein-2 Barycenter, minimizing the average discrepancy in terms of the Wasserstein-2 distance between the clients' distributions. A closed form solution for the Wasserstein Barycenter under Assumption 1 is obtained in [2]:

$$\Sigma_{W_2^2} = \left(\sum_{k=1}^N w_k \Sigma_k^{\frac{1}{2}} \right)^2, \quad \mu_{W_2^2} = \sum_{k=1}^N w_k \mu_k. \quad (4)$$

- The Reverse KL Barycenter, minimizing the average reverse KL divergences between the local distributions, coincides with the multiplicative aggregation of posteriors used in [1, 22, 36, 40]. Its statistics are obtained [31] as follows:

$$\Sigma_{RKL} = \left(\sum_{k=1}^N w_k \Sigma_k^{-1} \right)^{-1}, \quad (5)$$

$$\mu_{RKL} = \Sigma_{RKL} \sum_{k=1}^N w_k \Sigma_k^{-1} \mu_k. \quad (6)$$

To support the various aggregation strategies that operate on covariance matrices, and to avoid arbitrarily setting the effective sample size parameter in IVON, which ideally corresponds to the total dataset size, often unknown at the server, we consider a subclass of IVON that explicitly stores the covariance matrix and performs sampling directly from it instead of relying on the Hessian matrix. This is made possible by the relation [43]

$$\sigma^2 = \frac{1}{N(h + \delta)}, \quad (7)$$

which enables the covariance matrix to be computed from the Hessian, where σ^2 denotes the variance, N is the dataset size, h is the Hessian approximation, and δ is the weight decay term. In practice, the covariance matrix is first computed locally after estimating the Hessian. These local covariances are then aggregated on the server, and the resulting global covariance matrix is sent back to the clients, where it is used to reconstruct the updated local Hessians. Unlike previous work [40] that employed IVON but was restricted to RCLB aggregation due to its direct operation on the Hessian, our formulation enables a wider support for covariance-based aggregation strategies.

4. Personalization via Information-Geometric Projection

The main contribution of this work lies in the interpretation of the personalization problem as a projection problem. Given a divergence function, the objective is to project the global posterior p_g onto the projection set of the k^{th} client, defined as the sphere centered in the local posterior p_k and of radius r_k . Conceptually, the projection can be understood as identifying the distribution within the “local neighborhood of the client’s posterior that best aligns with the global model. In this setting, the radius r_k encodes the degree of personalization required by the client, where smaller values of r_k imply a stricter alignment to the local posterior rather than to the global model, as shown in Figure 1. In the following, we define a local sphere \mathcal{S}_k under a divergence function D .

Definition 1. (*Local Sphere $\mathcal{S}_D(p, r)$*) Given a statistical manifold \mathcal{M} and a divergence function D , the local sphere $\mathcal{S}_D(p, r)$ for $p \in \mathcal{M}$ and $r \in [0, \infty)$ is the set

$$\mathcal{S}_D(p, r) = \{q \in \mathcal{M} : D(q||p) \leq r\} \subseteq \mathcal{M}$$

To simplify the notation, we will indicate with $\mathcal{S}_k = \mathcal{S}_D(p_k, r_k)$ the local sphere of the k^{th} client centered in the local posterior p_k and of radius r_k . We are now ready to provide a formal definition of the personalization problem as a projection problem.

Problem 1. (*Projection on \mathcal{S}_k*) Given a statistical manifold \mathcal{M} , a divergence function D , a global posterior $p_g \in \mathcal{M}$, and a local sphere \mathcal{S}_k , we define the projection problem of p_g on \mathcal{S}_k as

$$\min_{p \in \mathcal{S}_k} D(p||p_g). \quad (8)$$

We identify the solution to this projection problem as the personalized posterior distribution $p_{g,k} = \arg \min_{p \in \mathcal{S}_k} D(p||p_g)$ of client k .

Remark 1. By varying the radius $r_k \in [0, D(p_k||p_g)]$, the solutions of the associated projection problem define the geodesic between p_k and p_g , i.e., the shortest possible path connecting the two distributions.

To support our derivation, we begin by presenting the definition of a barycenter with respect to a given divergence D .

Definition 2. (*D-barycenter*) Given a statistical manifold \mathcal{M} , a divergence function D , and a set of distributions $\{p_k\}_{k=1}^N \subseteq \mathcal{M}$ with associated normalized weights $\{w_k\}_{k=1}^N$, the barycenter of the set $\{p_k\}_{k=1}^N$ is defined as

$$p_D^*(\{p_k\}_{k=1}^N, \{w_k\}_{k=1}^N) = \arg \min_{q \in \mathcal{M}} \sum_{k=1}^N w_k D(q||p_k). \quad (9)$$

The following mild assumption is crucial for establishing the equivalence between the projection and barycenter problems, as shown in Theorem 1.

Assumption 2. *The divergence metric is a convex function in the first argument.*

Remark 2. *Most commonly used divergences, including the family of f -divergences and Wasserstein- p distances, are convex in both of their arguments.*

Theorem 1. *Given Assumption 2, the solution of the projection problem (8) is equivalent to the weighted barycenter problem (2), i.e.,*

$$p_{g,k} = p_D^*(\{p_g, p_k\}, \{w_g, w_k\}) \quad (10)$$

where w_g and w_k are defined as

$$w_g = \frac{1}{\lambda + 1}, \quad w_k = \frac{\lambda}{\lambda + 1} \quad (11)$$

for some $\lambda \in [0, \infty)$.

We highlight the following observations regarding the relationship between r_k and λ .

Remark 3. *There exists an inverse proportionality between the Lagrangian multiplier λ and the radius r_k . Specifically, as $\lambda \rightarrow 0$, the radius $r_k \rightarrow \infty$, corresponding to the case where the personalized posterior aligns with the global posterior. Conversely, in the limit $\lambda \rightarrow \infty$, the radius r_k vanishes ($r_k \rightarrow 0$), leading to the assignment of the local posterior to the personalized posterior. **Therefore, by selecting a λ we implicitly fix the personalization radius r_k .***

The main advantage of the equivalence between projections and barycenters lies in the greater tractability of the barycentric formulation. For example, under Assumption 1, analytical solutions exist for both the RKL divergence and the Wasserstein-2 distance, as shown in [2, 31]. These closed-form solutions enable a straightforward and computationally cost-free personalization process.

5. Experiments

5.1. Experimental Setting

Datasets and Heterogeneity Simulation We evaluate our approach on three widely used image classification benchmarks: FashionMNIST, SVHN, and CIFAR-10. To simulate the label shift across the 10 clients, we consider Dirichlet-based partitioning, where, similarly to prior works [33, 35, 39, 47, 48, 50], we sample client-specific label distributions from a Dirichlet distribution with concentration parameter $\beta = 0.5$, inducing non-i.i.d data across clients.

Model Architecture and Hyperparameters Our model architecture consists of two convolutional layers with 5×5 kernels and ReLU activations, each followed by a 2×2 max-pooling layer. The extracted features are flattened and passed through three fully connected layers of sizes 120, 84, and 10, respectively, to produce the final class logits. For all state-of-the-art methods we compare against, we closely adhere to the implementation details provided in the original papers. We note that the complexity of our architecture is similar to the models used in the selected state-of-the-art methods, ensuring a fair and consistent comparison. Whenever possible, we use the official codebases for implementation; otherwise, we carefully reproduce the setups following the authors’ guidelines to maintain alignment with their reported settings. We make an exception for pFedBayes on FashionMNIST, where, instead of the original Multi-Layer Perceptron model with one hidden layer, we use our architecture to produce a fair comparison.

Personalization Step For personalization, we restrict our experimental evaluation to the RKL and WB, as both barycenters preserve the Gaussian structure of the distributions. This preservation is a critical design choice, as it facilitates the adaptability of the personalized models. In

particular, it ensures that the posterior distribution of the personalized model remains aligned with those of both the global and local models, which are assumed to be Gaussian under the variational learning framework.

5.2. Comparison between the different aggregation methods considered

Our experiments investigate different combinations of global update methods (EAA, RKL, WB) and personalization techniques (RKL, WB). Statistical tests, provided in Appendix C, support our observation of comparable performance across these configurations. To reduce redundancy and enhance readability, we limit the results presented in the subsequent experiments to WB for both global updates and personalization.

5.3. Effect of λ on the trade-off between performance on local and global data

We analyze the impact of the personalization parameter λ on model performance across three datasets under heterogeneity simulated with the Dirichlet distribution. Across all datasets, we observe a consistent trade-off between performance on global and local data. Results on CIFAR-10 are reported in Figure 2. The global data, i.e., the union of all client test sets, is approximately uniform over classes while the local data follows different Dirichlet distributions. Notably, $\lambda = 0$ coincides with the global model, and $\lambda \rightarrow \infty$ corresponds to the local model. As λ increases, performance on the global distribution deteriorates in terms of accuracy, calibration (ECE), and uncertainty quantification (measured by NLL), whereas local performance improves and remains stable over a certain range of λ . The increased ECE and NLL for local models ($\lambda \rightarrow \infty$) on global data suggest that over-personalization may reduce generalization and model confidence, particularly for underrepresented classes. Conversely, at lower values of λ , the model achieves improved global performance but fails to effectively capture client-specific distributions and shows reduced confidence on local data. These results underscore the importance of λ in controlling the trade-off between generalization and personalization, enabling the model to adapt effectively to heterogeneous data distributions in non-i.i.d. federated settings.

5.4. Comparison with state-of-the-art

In this section, we provide a detailed analysis of the results presented in Table 1 and Figure 3. All reported values correspond to the mean and standard deviation over three independent runs.

Results of Personalized Models It is worth noting that all methods in the comparison, except FedAVG, employ personalized models. Consequently, we compare the local

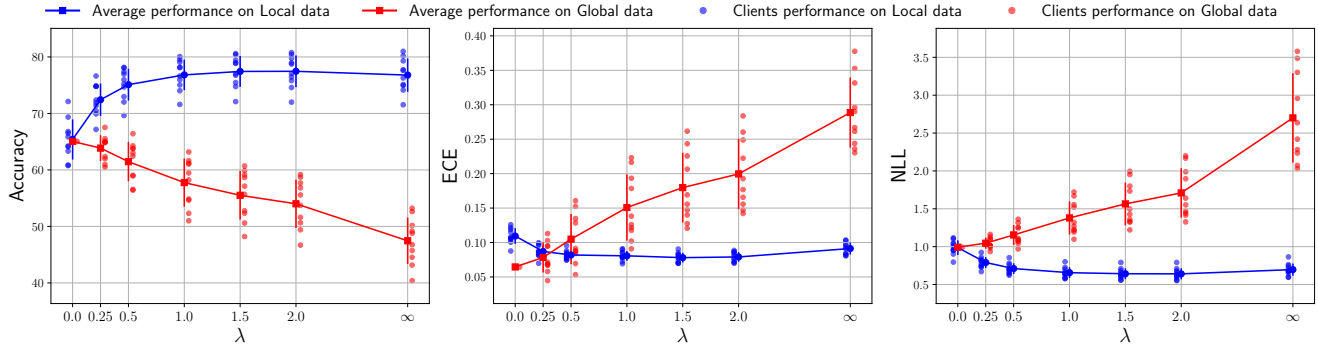


Figure 2. Effect of λ on the performance of local versus global data distributions. Results are reported for the CIFAR-10 dataset. Notably, $\lambda = 0$ corresponds to the global model and $\lambda \rightarrow \infty$ corresponds to the local model.

Table 1. Comparison of all methods across four evaluation settings: personalized models on local data (PM on LD), personalized models on global data (PM on GD), global models on local data (GM on LD), and global models on global data (GM on GD). Results are reported for three datasets (FashionMNIST, SVHN, CIFAR-10) using Accuracy, NLL, and ECE as evaluation metrics.

Setting	Method	FashionMNIST			SVHN			CIFAR-10		
		Acc	ECE	NLL	Acc	ECE	NLL	Acc	ECE	NLL
PM on LD	FedAVG	92.28 ± 3.16	0.07 ± 0.03	0.56 ± 0.26	91.17 ± 3.38	0.08 ± 0.03	0.74 ± 0.29	74.80 ± 4.89	0.13 ± 0.02	0.91 ± 0.16
	pFedBayes	91.42 ± 3.35	0.05 ± 0.01	0.25 ± 0.09	89.27 ± 3.27	0.07 ± 0.02	0.53 ± 0.19	71.84 ± 6.25	0.17 ± 0.04	1.10 ± 0.25
	FedPop	98.35 ± 0.37	0.02 ± 0.004	0.09 ± 0.02	89.77 ± 3.49	0.08 ± 0.03	0.74 ± 0.28	80.51 ± 4.66	0.07 ± 0.01	0.56 ± 0.12
	pFedVem	93.00 ± 2.80	0.06 ± 0.02	0.34 ± 0.14	91.69 ± 3.03	0.07 ± 0.02	0.55 ± 0.20	72.61 ± 5.09	0.23 ± 0.04	1.94 ± 0.42
	Ours ($\lambda = 1$)	92.22 ± 3.23	0.06 ± 0.02	0.34 ± 0.14	91.87 ± 3.03	0.05 ± 0.02	0.40 ± 0.14	76.82 ± 4.01	0.08 ± 0.01	0.66 ± 0.10
PM on GD	FedAVG	79.12 ± 5.56	0.18 ± 0.05	1.80 ± 0.68	68.67 ± 8.54	0.27 ± 0.08	3.11 ± 1.13	45.89 ± 6.78	0.36 ± 0.07	3.65 ± 1.24
	pFedBayes	77.51 ± 5.11	0.12 ± 0.05	0.78 ± 0.25	66.20 ± 10.71	0.26 ± 0.10	2.28 ± 1.04	44.48 ± 6.50	0.38 ± 0.08	3.12 ± 0.90
	FedPop	6.53 ± 0.49	0.82 ± 0.02	11.82 ± 0.78	60.00 ± 11.71	0.34 ± 0.12	4.92 ± 2.28	52.05 ± 8.00	0.25 ± 0.08	2.86 ± 1.54
	pFedVem	80.74 ± 5.17	0.15 ± 0.05	1.15 ± 0.46	67.92 ± 10.31	0.26 ± 0.10	2.55 ± 1.10	45.88 ± 6.05	0.46 ± 0.06	5.15 ± 1.22
	Ours ($\lambda = 1$)	84.61 ± 3.41	0.11 ± 0.03	0.73 ± 0.18	79.87 ± 5.21	0.12 ± 0.04	1.00 ± 0.31	57.75 ± 6.98	0.15 ± 0.07	1.38 ± 0.33
GM on LD	FedAVG	87.89 ± 4.83	0.10 ± 0.04	0.73 ± 0.29	86.62 ± 3.97	0.11 ± 0.03	0.98 ± 0.31	61.24 ± 7.67	0.16 ± 0.05	1.20 ± 0.25
	pFedBayes	88.00 ± 5.10	0.06 ± 0.02	0.34 ± 0.13	85.76 ± 6.11	0.09 ± 0.04	0.67 ± 0.32	63.85 ± 5.17	0.17 ± 0.03	1.25 ± 0.21
	FedPop	-	-	-	-	-	-	-	-	-
	pFedVem	89.49 ± 3.95	0.08 ± 0.03	0.45 ± 0.16	86.15 ± 4.74	0.10 ± 0.03	0.81 ± 0.28	60.98 ± 4.50	0.30 ± 0.04	2.43 ± 0.35
	Ours	88.45 ± 4.88	0.08 ± 0.03	0.47 ± 0.20	87.18 ± 4.63	0.07 ± 0.03	0.58 ± 0.20	65.39 ± 6.74	0.11 ± 0.02	0.99 ± 0.18
GM on GD	FedAVG	87.88 ± 0.97	0.09 ± 0.01	0.76 ± 0.05	86.06 ± 0.55	0.11 ± 0.01	1.01 ± 0.07	61.63 ± 3.81	0.12 ± 0.03	1.18 ± 0.13
	pFedBayes	88.02 ± 0.39	0.03 ± 0.005	0.34 ± 0.02	86.03 ± 0.41	0.08 ± 0.005	0.66 ± 0.04	63.86 ± 1.58	0.16 ± 0.01	1.25 ± 0.06
	FedPop	-	-	-	-	-	-	-	-	-
	pFedVem	89.50 ± 0.23	0.07 ± 0.002	0.45 ± 0.02	86.32 ± 0.22	0.09 ± 0.004	0.80 ± 0.03	60.88 ± 1.44	0.29 ± 0.01	2.44 ± 0.10
	Ours	88.14 ± 0.60	0.07 ± 0.004	0.49 ± 0.02	86.54 ± 1.05	0.06 ± 0.01	0.60 ± 0.06	65.05 ± 3.57	0.06 ± 0.01	0.99 ± 0.09

models of FedAVG, i.e., the models sent by the clients before aggregation, to the personalized models produced by the other methods, including ours. The results are presented in the first two groups of rows in Table 1 and Figure 3.

- *On Local Data:* Personalized models are designed to adapt to client-specific distributions, which is clearly reflected in their local accuracy scores, shown in the first group of rows in Table 1. Our method achieves perfor-

mance comparable to or better than the baselines; for example, it achieves the highest accuracy in SVHN and is second in CIFAR-10. In terms of calibration (ECE) and uncertainty quantification (NLL), our method consistently yields low error rates on local data, achieving the best performance in SVHN and second best in CIFAR-10.

- *On Global Data:* A key limitation of many personalized methods is the degradation in global performance due

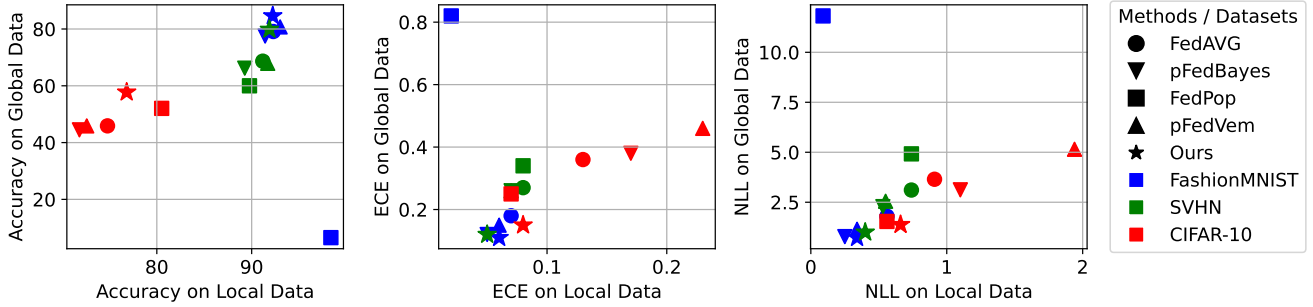


Figure 3. Trade-offs between local and global performance for personalized models. Each subplot shows results for a different evaluation metric: Accuracy (left), ECE (center), and NLL (right). Points represent method–dataset pairs. For accuracy, the top-right indicates a better performance trade-off; for ECE and NLL, the bottom-left is preferable. Our method (with $\lambda = 1$) consistently achieves a favorable balance across all metrics and datasets.

to overfitting to client-specific distributions. This trade-off is particularly evident in FedPop on FashionMNIST, where it achieves the best local accuracy, but performs poorly on global evaluations. In contrast, our method maintains strong generalization, achieving the highest global accuracy across all datasets: 84.61% on FashionMNIST, 79.87% on SVHN, and 57.75% on CIFAR-10. These represent improvements of 3.87%, 11.20%, and 5.70%, respectively, over the second-best method on each dataset. Furthermore, our method consistently achieves the lowest ECE and NLL on global data, demonstrating both well-calibrated predictions and effective uncertainty quantification.

- *Trade-off Analysis:* Figure 3 visualizes the trade-off between local and global performance for personalized models in the three metrics. For accuracy, the top-right region indicates favorable performance; for ECE and NLL, better performance lies in the bottom left. Our method consistently appears closest to the optimal region in all three plots, demonstrating strong local accuracy without sacrificing global generalization. The plots confirm that our method achieves a superior balance across all datasets, combining high accuracy with well-calibrated and confident predictions.

Results of Global Models We compare the performance of global models across all methods, excluding FedPop, which by design does not maintain a global model. The results discussed below correspond to the last two groups of rows in Table 1. The results for global models on both local and global data are closely similar, as the GM-on-LD setting reports the average performance of the global model evaluated across all clients’ local data. Our method performs strongly in the global setting, achieving the best results in SVHN and CIFAR-10, across all three metrics: accuracy, ECE, and NLL. This demonstrates not only high predictive performance but also well-calibrated and confi-

dent uncertainty estimates, highlighting the robustness of our approach even in non-personalized settings.

6. Conclusions

In this work, we proposed a personalized BFL method that balances local adaptation with global generalization, while explicitly accounting for uncertainty quantification and model calibration. Our approach combines variational learning with information-geometric tools, namely projection and barycenters, to produce client-specific models that remain robust under data heterogeneity, with minimal additional cost. Through experiments on three benchmark datasets, FashionMNIST, SVHN, and CIFAR-10, we demonstrate that our method consistently achieves a favorable trade-off between performance on local and global data distributions. In global evaluations, our personalized models outperform existing baselines in terms of accuracy, calibration, and uncertainty quantification, while also maintaining highly competitive performance in local data. This contrasts with other methods that tend to overfit or underfit across clients. Furthermore, we show that the global model produced by our approach generalizes relatively better than those of the compared state-of-the-art methods. These empirical results highlight the effectiveness of principled, information-geometric personalization combined with variational learning in federated settings. Future work includes exploring adaptive mechanisms to control the degree of personalization, extending our personalization method to non-parametric BFL, and evaluating its performance under additional heterogeneity scenarios, such as feature and quantity shifts.

Acknowledgments

The work has been supported by the EC through the Horizon Europe/JU SNS project, ROBUST-6G (Grant Agreement no. 101139068), the IMT "Futur, Ruptures & Im-

facts" program, and the European Research Council (ERC) under the European Union's Horizon 2020 Research and Innovation programme (Grant agreement No.101003431).

References

- [1] Maruan Al-Shedivat, Jennifer Gillenwater, Eric Xing, and Afshin Rostamizadeh. Federated Learning via Posterior Averaging: A New Perspective and Practical Algorithms. *arXiv preprint arXiv:2010.05273*, 2020. 2, 4
- [2] Pedro C Álvarez-Esteban, E Del Barrio, JA Cuesta-Albertos, and C Matrán. A Fixed-point Approach to Barycenters in Wasserstein Space. *Journal of Mathematical Analysis and Applications*, 441(2):744–762, 2016. 4, 6
- [3] Shun-ichi Amari. *Information Geometry and Its Applications*. Springer, 2016. 3
- [4] Manoj Ghuhan Arivazhagan, Vinay Aggarwal, Aaditya Kumar Singh, and Sunav Choudhary. Federated Learning with Personalization Layers. *arXiv preprint arXiv:1912.00818*, 2019. 1
- [5] Shrey Bhatt, Aishwarya Gupta, and Piyush Rai. Federated Learning with Uncertainty via Distilled Predictive Distributions. In *Asian Conference on Machine Learning*, pages 153–168. PMLR, 2024. 2, 4
- [6] Mahrokh Ghoddousi Boroujeni, Andreas Krause, and Giancarlo Ferrari Trecate. Personalized Federated Learning of Probabilistic Models: A PAC-Bayesian Approach. *arXiv preprint arXiv:2401.08351*, 2024. 1, 2
- [7] Longbing Cao, Hui Chen, Xuhui Fan, Joao Gama, Yew-Soon Ong, and Vipin Kumar. Bayesian Federated Learning: A Survey. *arXiv preprint arXiv:2304.13267*, 2023. 2
- [8] Hong-You Chen and Wei-Lun Chao. Fedbe: Making Bayesian Model Ensemble Applicable to Federated Learning. *arXiv preprint arXiv:2009.01974*, 2020. 2
- [9] Yiqiang Chen, Xin Qin, Jindong Wang, Chaohui Yu, and Wen Gao. Fedhealth: A Federated Transfer Learning Framework for Wearable Healthcare. *IEEE Intelligent Systems*, 35(4):83–93, 2020. 1
- [10] Luca Corinzia, Ami Beuret, and Joachim M Buhmann. Variational Federated Multi-task Learning. *arXiv preprint arXiv:1906.06268*, 2019. 2
- [11] Nicolas Courty, Rémi Flamary, Devis Tuia, and Alain Rakotomamonjy. Optimal Transport for Domain Adaptation. *IEEE transactions on pattern analysis and machine intelligence*, 39(9):1853–1865, 2016. 12
- [12] I. Csiszár. I -Divergence Geometry of Probability Distributions and Minimization Problems. *The Annals of Probability*, 3(1):146 – 158, 1975. 3
- [13] I. Csiszár and F. Matus. Information Projections Revisited. *IEEE Transactions on Information Theory*, 49(6):1474–1490, 2003. 3
- [14] Marco Cuturi. Sinkhorn Distances: Lightspeed Computation of Optimal Transport. *Advances in Neural Information Processing Systems*, 26, 2013. 3
- [15] Janez Demšar. Statistical Comparisons of Classifiers Over Multiple Data Sets. *Journal of Machine Learning Research*, 7(Jan):1–30, 2006. 11
- [16] Siddharth Divi, Yi-Shan Lin, Habiba Farrukh, and Z Berkay Celik. New Metrics to Evaluate the Performance and Fairness of Personalized Federated Learning. *arXiv preprint arXiv:2107.13173*, 2021. 3
- [17] Alessandro D’Ortenzio, Costanzo Manes, and Umut Orguner. Fixed-point Iterative Computation of Gaussian Barycenters for Some Dissimilarity Measures. In *2022 International Conference on Computational Science and Computational Intelligence (CSCI)*, pages 1422–1428, 2022. 3
- [18] Alireza Fallah, Aryan Mokhtari, and Asuman Ozdaglar. Personalized Federated Learning: A Meta-Learning Approach. *arXiv preprint arXiv:2002.07948*, 2020. 1
- [19] Farzan Farnia, Amirhossein Reiszadeh, Ramtin Pedarsani, and Ali Jadbabaie. An Optimal Transport Approach to Personalized Federated Learning. *IEEE Journal on Selected Areas in Information Theory*, 3(2):162–171, 2022. 4
- [20] John Fischer, Marko Orescanin, Justin Loomis, and Patrick McClure. Federated Bayesian Deep Learning: The Application of Statistical Aggregation Methods to Bayesian Models. *arXiv preprint arXiv:2403.15263*, 2024. 4
- [21] Wilfrid Gangbo and Andrzej Święch. Optimal Maps for the Multidimensional Monge-kantorovich Problem. *Communications on Pure and Applied Mathematics: A Journal Issued by the Courant Institute of Mathematical Sciences*, 51(1):23–45, 1998. 3
- [22] Han Guo, Philip Greengard, Hongyi Wang, Andrew Gelman, Yoon Kim, and Eric P Xing. Federated Learning As Variational Inference: A Scalable Expectation Propagation Approach. *arXiv preprint arXiv:2302.04228*, 2023. 2, 4
- [23] Mohsin Hasan, Guojun Zhang, Kaiyang Guo, Xi Chen, and Pascal Poupart. Calibrated One Round Federated Learning with Bayesian Inference in the Predictive Space. In *Proceedings of the AAAI conference on artificial intelligence*, pages 12313–12321, 2024. 2
- [24] Conor Hassan, Robert Salomone, and Kerrie Mengersen. Federated Variational Inference Methods for Structured Latent Variable Models. *arXiv preprint arXiv:2302.03314*, 2023. 4
- [25] Nour Jamoussi, Giuseppe Serra, Photios A Stavrou, and Marios Kountouris. Information-Geometric Barycenters for Bayesian Federated Learning. *arXiv preprint arXiv:2412.11646*, 2024. 2, 4
- [26] Eunjeong Jeong and Marios Kountouris. Personalized Decentralized Federated Learning with Knowledge Distillation. In *ICC 2023 - IEEE International Conference on Communications*, pages 1982–1987, 2023. 1
- [27] Rahif Kassab and Osvaldo Simeone. Federated Generalized Bayesian Learning via Distributed Stein Variational Gradient Descent. *IEEE Transactions on Signal Processing*, 70: 2180–2192, 2022. 2
- [28] Mohammad Emtiyaz Khan and Håvard Rue. The Bayesian Learning Rule. *arXiv preprint arXiv:2107.04562*, 2021. 4
- [29] Minyoung Kim and Timothy Hospedales. Fedhb: Hierarchical Bayesian Federated Learning. *arXiv preprint arXiv:2305.04979*, 2023. 2
- [30] James Kirkpatrick, Razvan Pascanu, Neil Rabinowitz, Joel Veness, Guillaume Desjardins, Andrei A Rusu, Kieran

- Milan, John Quan, Tiago Ramalho, Agnieszka Grabska-Barwinska, et al. Overcoming Catastrophic Forgetting in Neural Networks. *Proceedings of the national academy of sciences*, 114(13):3521–3526, 2017. 12
- [31] Günther Koliander, Yousef El-Laham, Petar M Djurić, and Franz Hlawatsch. Fusion of Probability Density Functions. *Proceedings of the IEEE*, 110(4):404–453, 2022. 4, 6
- [32] Nikita Kotelevskii, Maxime Vono, Alain Durmus, and Eric Moulines. Fedpop: A Bayesian Approach for Personalised Federated Learning. *Advances in Neural Information Processing Systems*, 35:8687–8701, 2022. 1, 2
- [33] Qinbin Li, Bingsheng He, and Dawn Song. Practical One-shot Federated Learning for Cross-silo Setting. *arXiv preprint arXiv:2010.01017*, 2020. 6
- [34] Wenqian Li, Shuran Fu, and Yan Pang. Distributionally Robust Federated Learning with Wasserstein Barycenter. In *The Second Tiny Papers Track at ICLR 2024*, 2024. 4
- [35] Tao Lin, Lingjing Kong, Sebastian U Stich, and Martin Jaggi. Ensemble Distillation for Robust Model Fusion in Federated Learning. *Advances in Neural Information Processing Systems*, 33:2351–2363, 2020. 6
- [36] Liangxi Liu, Xi Jiang, Feng Zheng, Hong Chen, Guo-Jun Qi, Heng Huang, and Ling Shao. A Bayesian Federated Learning Framework with Online Laplace Approximation. *IEEE Transactions on Pattern Analysis and Machine Intelligence*, 2023. 2, 4
- [37] Brendan McMahan, Eider Moore, Daniel Ramage, Seth Hampson, and Blaise Agueria y Arcas. Communication-efficient Learning of Deep Networks From Decentralized Data. In *Artificial intelligence and statistics*, pages 1273–1282. PMLR, 2017. 1
- [38] Frank Nielsen and Richard Nock. Sided and Symmetrized Bregman Centroids. *IEEE Transactions on Information Theory*, 55(6):2882–2904, 2009. 3
- [39] Atahan Ozer, Kadir Burak Buldu, Abdullah Akgül, and Gozde Unal. How to Combine Variational Bayesian Networks in Federated Learning. *arXiv preprint arXiv:2206.10897*, 2022. 2, 4, 6
- [40] Shivam Pal, Aishwarya Gupta, Saqib Sarwar, and Piyush Rai. Simple and Scalable Federated Learning with Uncertainty via Improved Variational Online Newton. In *OPT 2024: Optimization for Machine Learning*, 2024. 2, 4, 5
- [41] Brendan Pass. Multi-Marginal Optimal Transport: Theory and Applications. *ESAIM: Mathematical Modelling and Numerical Analysis*, 49(6):1771–1790, 2015. 3
- [42] Felix Sattler, Klaus-Robert Müller, and Wojciech Samek. Clustered Federated Learning: Model-Agnostic Distributed Multitask Optimization Under Privacy Constraints. *IEEE Transactions on Neural Networks and Learning Systems*, 32(8):3710–3722, 2020. 1
- [43] Yuesong Shen, Nico Daheim, Bai Cong, Peter Nickl, Gian Maria Marconi, Clement Bazan, Rio Yokota, Iryna Gurevych, Daniel Cremers, Mohammad Emtiyaz Khan, et al. Variational Learning Is Effective for Large Deep Networks. *arXiv preprint arXiv:2402.17641*, 2024. 2, 4, 5
- [44] Siddharth Swaroop, Mohammad Emtiyaz Khan, and Finale Doshi-Velez. Connecting Federated ADMM to Bayes. *arXiv preprint arXiv:2501.17325*, 2025. 2
- [45] Alysa Ziyang Tan, Han Yu, Lizhen Cui, and Qiang Yang. Towards Personalized Federated Learning. *IEEE Transactions on Neural Networks and Learning Systems*, 34(12):9587–9603, 2023. 1
- [46] Cédric Villani. *Optimal Transport: Old and New*. Springer, 2009. 3
- [47] Hongyi Wang, Mikhail Yurochkin, Yuekai Sun, Dimitris Papailiopoulos, and Yasaman Khazaeni. Federated Learning with Matched Averaging. *arXiv preprint arXiv:2002.06440*, 2020. 6
- [48] Jianyu Wang, Qinghua Liu, Hao Liang, Gauri Joshi, and H Vincent Poor. Tackling the Objective Inconsistency Problem in Heterogeneous Federated Optimization. *Advances in Neural Information Processing Systems*, 33:7611–7623, 2020. 6
- [49] Miao Yang, Ximin Wang, Hongbin Zhu, Haifeng Wang, and Hua Qian. Federated Learning with Class Imbalance Reduction. In *2021 29th European Signal Processing Conference (EUSIPCO)*, pages 2174–2178. IEEE, 2021. 1
- [50] Mikhail Yurochkin, Mayank Agarwal, Soumya Ghosh, Kristjan Greenewald, Nghia Hoang, and Yasaman Khazaeni. Bayesian Nonparametric Federated Learning of Neural Networks. In *International Conference on Machine Learning*, pages 7252–7261. PMLR, 2019. 2, 6
- [51] Xu Zhang, Yinchuan Li, Wenpeng Li, Kaiyang Guo, and Yunfeng Shao. Personalized Federated Learning via Variational Bayesian Inference. In *International Conference on Machine Learning*, pages 26293–26310. PMLR, 2022. 1, 2, 3, 4
- [52] Junyi Zhu, Xingchen Ma, and Matthew B Blaschko. Confidence-aware Personalized Federated Learning via Variational Expectation Maximization. In *Proceedings of the IEEE/CVF Conference on Computer Vision and Pattern Recognition*, pages 24542–24551, 2023. 1, 2, 3

A. Proof of Theorem 1

Proof. Under Assumption 2, (8) is a convex optimization problem. Therefore, we can apply Lagrangian duality to the projection problem. For a fixed Lagrangian multiplier λ , the minimization problem becomes

$$\min_{p \in \mathcal{M}} \mathcal{L}_\lambda(p), \quad \text{where } \mathcal{L}_\lambda(p) = D(p||p_g) + \lambda D(p||p_k).$$

We can rewrite $\mathcal{L}_\lambda(p)$ as

$$\mathcal{L}_\lambda(p) = (\lambda + 1) \left(\frac{1}{\lambda + 1} D(p||p_g) + \frac{\lambda}{\lambda + 1} D(p||p_k) \right).$$

Let w_g, w_k be defined as in (11). Then, the minimization problem becomes

$$\min_{p \in \mathcal{M}} w_g D(p||p_g) + w_k D(p||p_k). \quad (12)$$

By Definition 2, the probability distribution p minimizing the weighted sum in (12) coincides with the D -Barycenter. This concludes the proof. \square

B. IVON Hyperparameters

It is worth noting that training with IVON can be sensitive to hyperparameters, particularly the initialization of the Hessian. To ensure reproducibility, we provide in Table 2 the hyperparameters used for each dataset. Here, N_k denotes the size of the training dataset of the k^{th} client.

Table 2. IVON Hyperparameters.

params	FashionMNIST	SVHN	CIFAR-10
initial learning rate	0.1	0.1	0.1
final learning rate	0.01	0.01	0.01
weight decay	2e-4	2e-4	2e-4
batch size	64	64	64
ESS	N_k	N_k	N_k
initial hessian (h_0)	5	2	1
MC sample while training	1	1	1
MC sample while testing	10	10	10

C. Comparison between the different aggregation methods considered

We conduct experiments with various combinations of global update and personalization methods, including EAA, RKLB, and WB for global aggregation, and RKLB and WB for personalization. Across all configurations, we observed consistent trends and similar results. To confirm our observations, we apply the Wilcoxon signed-rank test [15] to compare the performance of different aggregation methods across multiple runs (seeds) and datasets. We compute pairwise Wilcoxon tests between all methods to assess whether

their performance differences are statistically significant. This allows us to build a matrix of p -values showing, for each pair of methods, whether one consistently outperforms the other. The results of the Wilcoxon signed-rank tests presented in Figure 4 show that, in most cases, the p -values are high, indicating no statistically significant difference between the aggregation methods. This suggests that, despite small fluctuations in performance across datasets, the aggregation methods perform similarly overall, and no single aggregation approach consistently outperforms the others in a statistically meaningful way for the different metrics considered. Additionally, to illustrate the variability and stability of the aggregation methods across different datasets, we provide violin plots in Figure 5. These plots show the distribution of global model accuracies across multiple random seeds for each aggregation method on FashionMNIST, SVHN, and CIFAR-10. The shape and spread of the distributions offer insights into both the typical performance (median) and variability (spread) of each method. Based on the violin plots, which show that the WB-based aggregation achieves competitive and consistently stable performance across datasets, we restrict the presentation of the experiments reported in the experimental part to this method for both the global update and personalization steps.

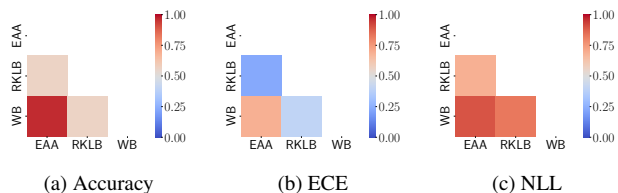


Figure 4. Wilcoxon rank-sum test p -values comparing aggregation methods across all datasets for three evaluation metrics: (a) Accuracy, (b) ECE, and (c) NLL. Lower p -values indicate statistically significant differences between methods. Only the lower triangle of each matrix is shown to avoid redundancy.

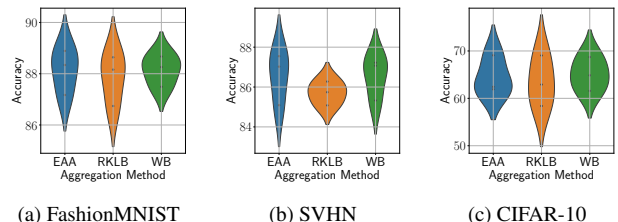


Figure 5. Accuracy distributions across seeds for different aggregation methods on: (a) FashionMNIST, (b) SVHN, and (c) CIFAR-10 datasets. Lower spread and higher median indicate better and more stable performance.

D. Beyond Federated Learning: Broader Applicability of the Proposed Method

While the use of Information Geometry in BFL is natural, our method also applies to any optimization over probability spaces rather than point estimates. The method can lend itself to domain adaptation: When a model is trained on source data A , and new target data B becomes available, re-training only on B may lead to catastrophic forgetting of the source domain. Our projection framework offers a principled trade-off, retaining prior knowledge while integrating new information. This is further enhanced by the flexibility of our method. In particular, the use of IVON combines the efficiency of deterministic learning with the ability to perform inference and adaptation in the posterior space. However, it is important to note that our approach fundamentally differs from standard domain adaptation methods based on optimal transport [11], which operate on data distributions rather than model posteriors.

Application in Incremental Learning We design a toy example to simulate an incremental learning scenario involving two sequential tasks:

- Task A, consisting of the first five classes of MNIST.
- Task B, corresponding to the remaining five classes.

We first train a model (Model A) on Task A. Subsequently, Task B becomes available, while access to Task A is revoked, mimicking a typical continual learning setup where previously seen data may no longer be accessible due to constraints such as data retention policies or regulations like the General Data Protection Regulation (GDPR). We evaluate multiple strategies: training a new model (Model B) solely on Task B, fine-tuning Model A on Task B with and without Elastic Weight Consolidation (EWC) [30], and computing the barycenters of Model A and Model B. As shown in Figure 6, barycentric combinations offer a favorable trade-off between the two tasks, preserving accuracy on Task A while effectively adapting to Task B. This mitigates the catastrophic forgetting observed in alternative approaches.

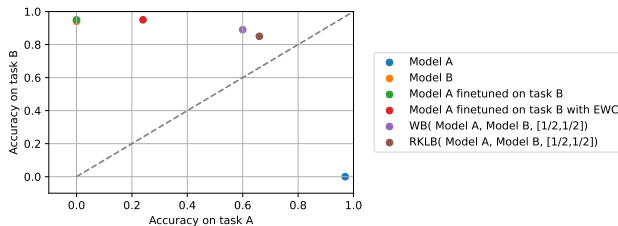


Figure 6. Accuracy Trade-off in an Incremental Learning Setting